applied sciences

MDPI

Article

Near-Field-Based 5G Sub-6 GHz Array Antenna Diagnosis Using Transfer Learning

Hong Jun Lim [1], Dong Hwan Lee [1], Hark Byeong Park [2] and Keum Cheol Hwang [1,*]

[1] Department of Electrical and Computer Engineering, Sungkyunkwan University, Suwon 440-746, Korea; zpeac@skku.edu (H.J.L.); excalibur7@skku.edu (D.H.L.)
[2] Global Technology Center, Samsung Electronics Co., Ltd., Suwon 443-742, Korea; hb111.park@samsung.com
* Correspondence: khwang@skku.edu; Tel.: +82-31-290-7978

Abstract: In this paper, we propose a method for near-field-based 5G sub 6-GHz array antenna diagnosis using transfer learning. A classification network was implemented for normal/abnormal operation of the array antenna and the failure of a specific port. Furthermore, a regression network that could predict the amplitude and phase of the excitation signal of the array antenna was employed. Additionally, to accelerate the array antenna diagnosis, several near-field lines were sampled and reflected in the regression network. The proposed method was verified by measuring a fabricated 5G sub-6 GHz band 4×4 array antenna in various scenarios using a divider and coaxial cables. The tests showed that the trained network accurately diagnosed 29 of 30 measurement results.

Keywords: near-field measurement; machine learning; transfer learning; array antenna diagnosis; 5G sub 6-GHz

check for updates

Citation: Lim, H.J.; Lee, D.H.; Park, H.B.; Hwang, K.C. Near-Field-Based 5G Sub-6 GHz Array Antenna Diagnosis Using Transfer Learning. *Appl. Sci.* **2021**, *11*, 10164. https://doi.org/10.3390/app112110164

Academic Editor: Hosung Choo

Received: 3 September 2021
Accepted: 26 October 2021
Published: 29 October 2021

Publisher's Note: MDPI stays neutral with regard to jurisdictional claims in published maps and institutional affiliations.

Copyright: © 2021 by the authors. Licensee MDPI, Basel, Switzerland. This article is an open access article distributed under the terms and conditions of the Creative Commons Attribution (CC BY) license (https://creativecommons.org/licenses/by/4.0/).

1. Introduction

Recently, with the expansion of the 5G mobile communication business, there has been a rapid increase in the demand for both single antennas, which are used in existing mobile phones, and array antennas, which have high gain and beam steering [1,2]. An array antenna consists of radiation elements and electronic components for controlling transmission and reception signals. It adjusts the amplitude and phase of the signal applied to each radiation element differently, and it subsequently steers the beam based on the principle of combination and cancellation of the radiation signals of the individual radiation elements [3]. In general, although an array antenna is composed of the same radiation elements and electronic components, the amplitude and phase errors of the applied signal are caused by problems such as component failure, mutual interference, and heat generation [4]. As these errors affect the performance of an array antenna, its diagnosis is essential.

Array antenna diagnosis methods are primarily classified as far-field and near-field methods. A far-field diagnosis based on the three-dimensional one-point measurement method has high accuracy; however, the measurement time is long, and the economic feasibility is low. The latter is a result of the requirement of an expensive, large-scale method, such as an electromagnetic wave anechoic chamber that can provide a far-field area. A near-field diagnosis method measures the electric field at regular intervals on an arbitrary plane in a radiating near-field of the antenna to be tested. Under modal expansion, the magnitude and phase of the angular spectrum of the plane wave can be determined from the measured near field [5]. Specifically, the electric field at any position can be calculated, and this method is called the back-projection technique. If this technique is applied to the surface of an array antenna, the electric field distribution near the surface can be predicted, and the correction/error, amplitude, and phase error can be determined in units of the array antenna elements. However, this technique is effective when more than a

certain amount of the energy radiated by the array antenna can be measured [6]. The back-projection technique requires measurements in a radiating near-field at a certain distance from the array antenna. Thus, a wide-area near-field measurement is required, which increases the measurement time. This means there is a trade-off relationship between the measurement time and the accuracy. In addition, because the resolution of the electric-field distribution image of an array antenna surface obtained by the back-projection technique is one wavelength interval, it is difficult to diagnose a particular antenna element when the antenna elements are dense. Therefore, it is difficult to obtain high accuracy and a short measurement time with the conventional array antenna diagnosis method [7]. To overcome these shortcomings, in this paper, we propose an array antenna diagnosis method by applying the imaged electric-field distribution to a convolutional neural network (CNN) [8].

Recently, the field of computer vision has rapidly developed with deep learning technology. In particular, the CNN method has led to breakthroughs in image recognition, classification, extraction, and tracking based on big data images, such as ImageNet [9]. Moreover, its performance has also been significantly improved, and it has been commonly used in various fields. To employ a general CNN, a developer must implement all layers directly and derive a CNN structure that is suitable for the target purpose by repeated training. However, this method requires high skills and is also inefficient in terms of the time and the computational cost. As an alternative, transfer learning [10], which trains a new model using the weights of a pre-trained deep learning model, has recently received significant attention. It is being applied in various fields, such as medicine, engineering, and agriculture, owing to the easy generation of information suitable for a new purpose using previously acquired information [11–13].

In this study, we aimed to diagnose a 5G sub-6-GHz array antenna based on a near field using transfer learning. A trained network based on the near field implemented the array antenna diagnosis technique with high accuracy and a short measurement time. First, the possibility of its diagnosis was reviewed by applying a classification network, and the amplitude and phase of the array antenna excitation signal were accurately predicted by implementing a regression network for the subsequent complete diagnosis. Additionally, to accelerate the measurements, a regression network was trained using the sampled near-field. The measurements verified the validity of the array antenna diagnosis by transfer learning. The remaining paper is organized as follows. The transfer learning and training data formation are introduced in Section 2, and the experimental results for the trained networks are presented in Section 3. Section 4 discusses the effectiveness of the array antenna diagnosis using transfer learning based on measurements on a fabricated array antenna, and finally, Section 5 presents the conclusion.

2. Research Method

2.1. Transfer Learning

A CNN is a type of artificial neural network used to analyze visual characteristics such as edges and textures of images, and it is made deep by repeatedly placing convolution and pooling layers and finally implementing a fully connected layer. A convolution layer extracts the image features by the convolution operation, and a pooling layer reduces the dimension using the average and maximum values in the filter size. Moreover, the fully connected layer connects the extracted features to create a feature map and classifies the image using a function. However, because a CNN contains various variables, such as initial value, activation function, number of layers, learning rate, and batch size, numerous factors need to be considered. To compensate this shortcoming, transfer learning was devised. Briefly, the concept of transfer learning originated from the problem of slow learning when training from scratch a very large deep learning model. In this case, the learning can be accelerated by introducing and reusing the lower layer of a similar pre-trained model [10]. Figure 1 shows the concept diagram of the transfer learning method employed in this study. For CNN models trained on ImageNet, the convolution kernels are set suitably for object

classification. In the pre-trained model trained on ImageNet, the output of the last stage is set to classify 1000 classes. The transfer learning can be performed if only the classification layer, i.e., the last stage, is supplemented and modified to enable the classification of the data desired by the user. In this study, Alexnet [14] and Resnet-50 [15] were used as the pre-trained networks; the classification layers of these networks were changed for the purpose of the array antenna diagnosis.

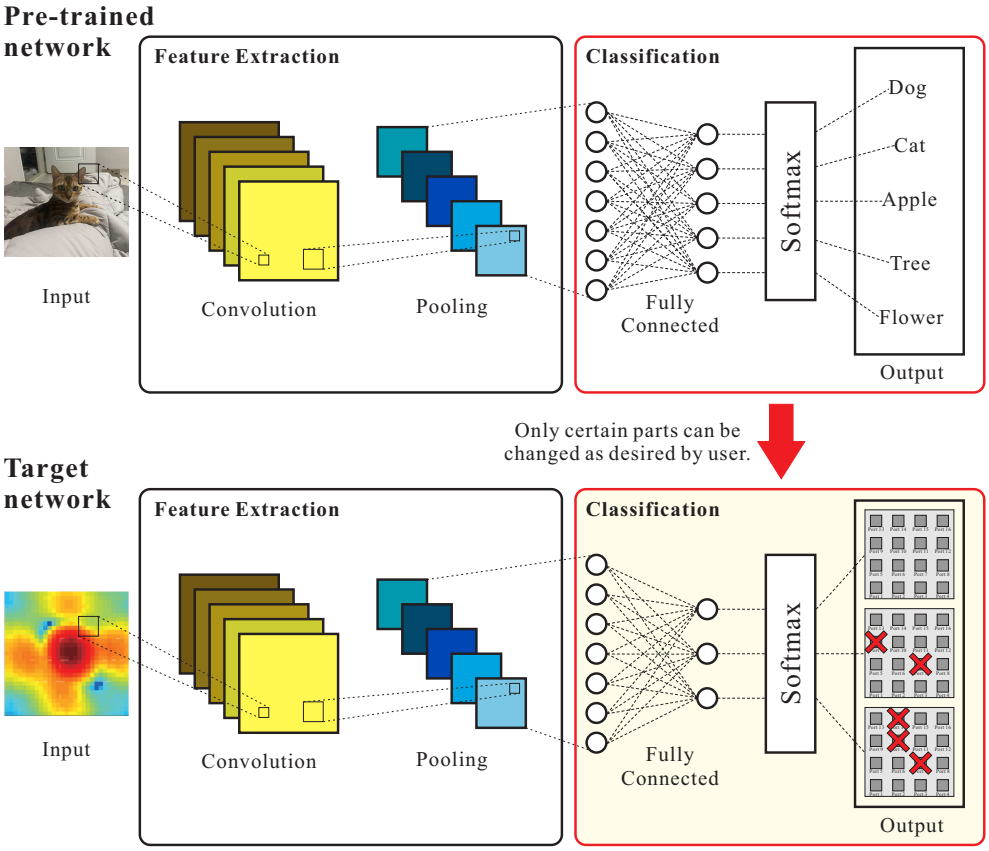

Figure 1. Concept diagram of transfer learning.

2.2. Preparation of training

As mentioned earlier, the classification layer of the pre-trained network is modified according to the purpose of the user and used as transfer learning. Table 1 shows the structure of Alexnet implemented in MATLAB. Alexnet consists of five convolutional layers and three fully connected layers. In five convolution layers, feature maps are extracted with the filter kernel and activated with the ReLU function. Through intermediate normalization, max pooling, etc., a $6 \times 6 \times 256$ feature map is finally obtained. Then, two fully connected layers convert the $6 \times 6 \times 256$ feature map into a one-dimensional form and connect it to 4096 neurons. This is the step of feature extraction from Alexnet. Only subsequent layers are modified to suit the purpose. The user changes the number of neurons in the third fully connected layer (layer 23 in Table 1), which consists of 1000 neurons, and also modifies the output layer (layer 25 in Table 1) to the corresponding class. If the specific port failure diagnosis of Section 3.2 described later is applied, layer 23 is modified to a fully connected layer composed of 17 neurons, and layer 25 is modified to corresponding classes such as pass, port 1 failure, etc.

Table 1. Structure of Alexnet implemented on MATLAB.

Layer	Name	Role	Note
1	'data'	Image Input	227 × 227 × 3 images with 'zerocenter' normalization
2	'conv1'	Convolution	96 11 × 11 × 3 convolutions with stride [4 4] and padding [0 0 0 0]
3	'relu1'	ReLU	ReLU
4	'norm1'	Cross Channel Normalization	Cross channel normalization with 5 channels per element
5	'pool1'	Max Pooling	3 × 3 max pooling with stride [2 2] and padding [0 0 0 0]
6	'conv2'	Convolution	256 5 × 5 × 48 convolutions with stride [1 1] and padding [2 2 2 2]
7	'relu2'	ReLU	ReLU
8	'norm2'	Cross Channel Normalization	Cross channel normalization with 5 channels per element
9	'pool2'	Max Pooling	3 × 3 max pooling with stride [2 2] and padding [0 0 0 0]
10	'conv3'	Convolution	384 3 × 3 × 256 convolutions with stride [1 1] and padding [1 1 1 1]
11	'relu3'	ReLU	ReLU
12	'conv4'	Convolution	384 3 × 3 × 192 convolutions with stride [1 1] and padding [1 1 1 1]
13	'relu4'	ReLU	ReLU
14	'conv5'	Convolution	384 3 × 3 × 192 convolutions with stride [1 1] and padding [1 1 1 1]
15	'relu5'	ReLU	ReLU
16	'pool5'	Max Pooling	3 × 3 max pooling with stride [2 2] and padding [0 0 0 0]
17	'fc1'	Fully Connected	4096 fully connected layer
18	'relu6'	ReLU	ReLU
19	'drop6'	Dropout	50% dropout
20	'fc2'	Fully Connected	4096 fully connected layer
21	'relu7'	ReLU	ReLU
22	'drop7'	Dropout	50% dropout
23	**'fc3'**	**Fully Connected**	**1000 fully connected layer**
24	'prob'	Softmax	Softmax
25	**'output'**	**Classification Output**	**Crossentropyex with 'tench', 'goldfish', and 998 other classes**

As input data, near-field data are required. However, it takes considerable time and financial resources to obtain more than thousands of sample data by measurements; thus, it is practically impossible to obtain sample data. Therefore, a realistic method is to obtain the sample data required for training from simulation, instead of measurements. In this study, near-field data based on the change in the excitation signal were used through a combination of post-processing results of the CST microwave studio (MWS). This allows collecting near-field data of an array antenna within a few seconds by a simple post-processing as well as reduces the time and cost for obtaining a sample database. The sample database was secured by linking MATLAB and CST MWS [16]. The labeling of the input data was implemented in MATLAB, and the near-field data were calculated through a combination of post-processing results after applying an excitation signal in CST MWS corresponding to the labeling. After re-importing the calculated near-field data in MATLAB, the sample data were obtained by adding the above data to the database.

Near-field data were extracted from the CST MWS environment, as shown in Figure 2. A 4 × 4 patch array antenna with radiating elements arranged at 0.5λ intervals was used as the antenna under test (AUT), and the operating frequency of the array antenna was 3.55 GHz in the 5G sub-6 GHz band. The area surrounding the array antenna at a distance of 1λ (84.5 mm) was extracted at a distance of 3λ (243.5 mm) above the array antenna. The total area was 330 × 330 mm^2, and the interval between the sample points was set as 10 mm. The total number of sample points extracted was 34 × 34. The data were extracted from a computer environment with Intel i5-9400F CPU and 16 GB RAM, and approximately 9.2 s was required for each datum.

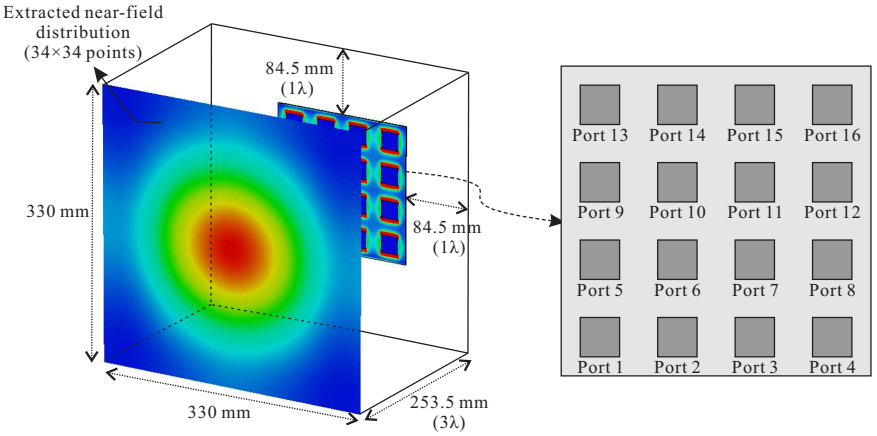

Figure 2. Near-field data extraction simulation environment in CST MWS.

3. Experiments with Simulation-Based Data

The experiments were conducted on a PC equipped with a 3.6 GHz CPU (Intel core i7-7820X), 128 GB RAM, and NVIDIA Quadro P6000 GPU, and CNN models were implemented and learned using MATLAB Deep Learning Toolbox. The datasets were divided and used for training, validation, and testing in the ratio of 7:1:2, respectively. For classification, Alexnet was used as the pre-trained network, and for regression, Alexnet and Resnet-50 were used as the pre-trained networks.

3.1. Classification of Normal/Abnormal Operations of Array Antenna

First, uniform excitation of the array antenna ($0.9 <$ amplitude ≤ 1, $-10^\circ <$ phase $< 10^\circ$ for all port excitation signals) was assumed to be its normal operation, and all other cases were assumed to be abnormal (See Table 2). An example of the near field according to the conditions is shown in Figure 3. For the near-field image, only the co-polarization component of the antenna was used. The amplitude of the near field was normalized to the maximum value when the uniform signals were excited to all ports, and the amplitude and the phase distribution image were arranged in parallel (left: amplitude, right: phase) as input image data. A total of 10,000 data were obtained by extracting 5000 normal data and 5000 abnormal data. The stochastic gradient descent method was used as the optimization algorithm, and the learning rate was set as 0.001. A maximum of 100 epochs were trained, and the batch size was set as 128.

Table 2. Normal/abnormal classification criteria for array antennas.

Normal	When $0.9 <$ amplitude ≤ 1, $-10^\circ <$ phase $< 10^\circ$ for all port excitation signals
Abormal	When $0.9 <$ amplitude ≤ 1, $-10^\circ <$ phase $< 10^\circ$ for any port excitation signal is not satisfied

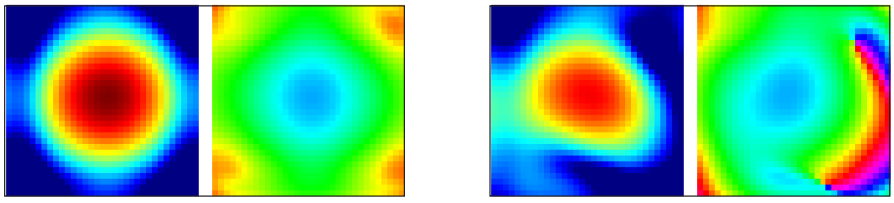

(a) (b)

Figure 3. Examples of near-field data in case of (**a**) normal and (**b**) abnormal operations.

The total training time was 1 h 07 min 46 s, and the accuracy of the network for 2000 test data was 99.6% (1992/2000). The minimum number of sample data for normal/abnormal diagnosis was determined by reducing the data for each class at the same rate. Table 3

shows a comparison of the accuracy and execution time of the trained network by the number of sample data while maintaining the training option. The accuracy reaches approximately 99% or more, and the minimum number of sample data that achieves 99% accuracy is 1000. Therefore, for normal/abnormal diagnosis of the 4×4 array antenna, the accuracy of the network can be ensured with only 1000 sample data.

Table 3. Normal/abnormal diagnosis result of array antenna by number of sample data.

	Number of Sample Data				
	500	**1000**	**3000**	**5000**	**10,000**
Accuracy	86.0%	99.0%	99.5%	99.2%	99.6%
Execution time	0 h 03 m 09 s	0 h 07 m 10 s	0 h 21 m 15 s	0 h 35 m 22 s	1 h 07 m 46 s

3.2. Classification of the Failure of Specific Port of Array Antenna

Specific failure port diagnosis of the array antenna was conducted in the same environment as that for its normal/abnormal diagnosis. The excitation signal of a specific port was assumed to be normal when the amplitude exceeded 0.9 and the phase ranged from -10° to 10°, and when all ports satisfied the normal condition, the case was assumed to be passed. When many ports were assumed to fail, the number of cases became extremely large. Thus, data were extracted by assuming failure for only one port; the network has 17 classification classes. The details are provided in Table 4. Examples of the near-field distribution for a specific port failure are shown in Figure 4. A total of 19,000 samples were obtained by extracting 3000 sample data for the pass case and 1000 samples for each 16 failure port cases.

Table 4. Specific port failure classification criteria for array antennas.

	Port 1	**Port 2**	**Port 3**	**Port 4**	…	**Port 16**
Pass	Normal	Normal	Normal	Normal	…	Normal
Port 1 Failure	Abnormal	Normal	Normal	Normal	…	Normal
Port 2 Failure	Normal	Abnormal	Normal	Normal	…	Normal
…	…	…	…	…	…	…
Port 16 Failure	Normal	Normal	Normal	Normal	…	Abnormal

The total training time was 2 h 15 min 57 s, and the accuracy of the specific failure port diagnosis network for 3800 test data was 95.24% (3619/3800). While reducing the pass and failure data for each port at the same rate, the minimum number of sample data that can diagnose a specific failure device was obtained. To this end, the training option was maintained, and the accuracy of the trained network by the number of sample data was compared (see Table 5). The accuracy reached approximately 95% or more, and the minimum number of sample data that achieved 95% accuracy was 10,000.

Table 5. Specific port failure diagnosis results for array antenna by number of sample data.

	Number of Sample Data				
	3000	**5000**	**10,000**	**15,000**	**19,000**
Accuracy	91.04%	92.11%	95.00%	94.60%	95.24%
Execution time	0 h 18 m 47 s	0 h 31 m 55 s	1 h 04 m 46 s	1 h 37 m 07 s	2 h 15 m 57 s

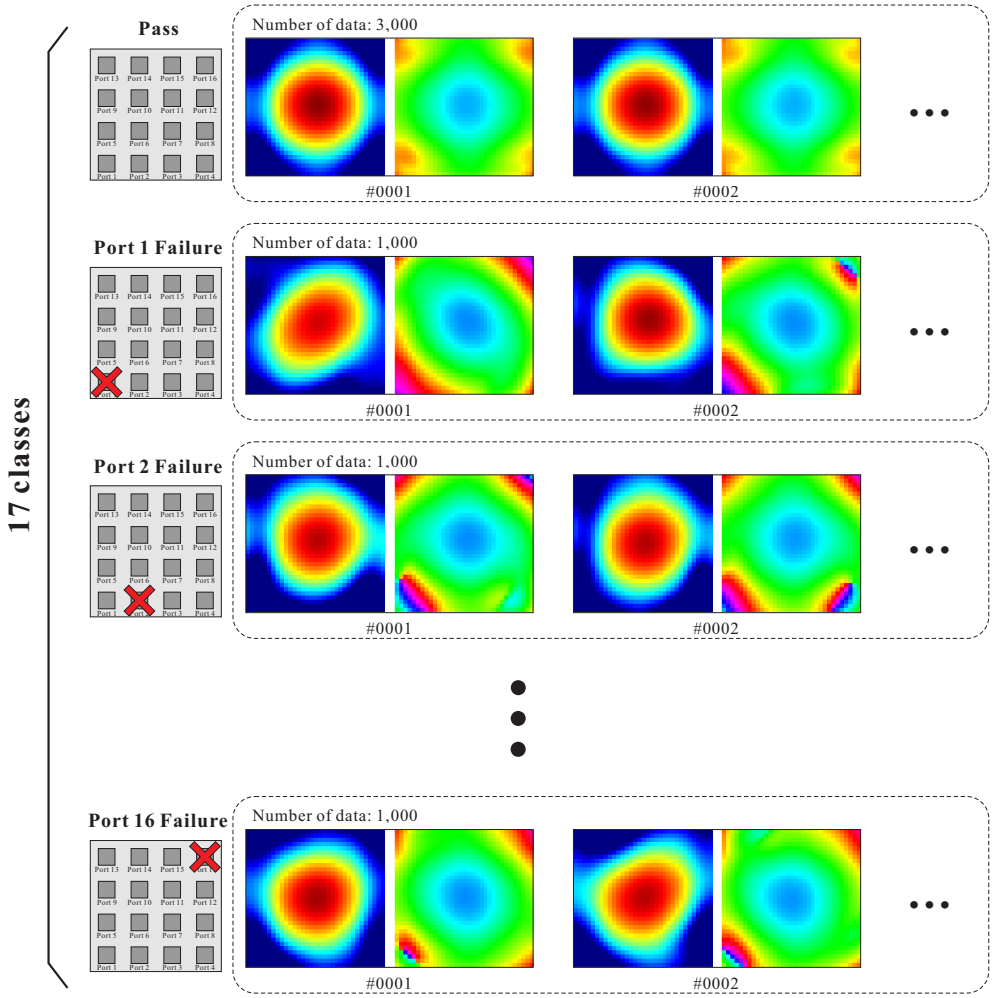

Figure 4. Dataset configuration of specific port failure diagnosis.

3.3. Regression of Excitation Signal Amplitude and Phase of Array Antenna

The assumption of failure of each port for the diagnosis of the 4×4 array antenna is very difficult to reflect in reality, owing to the numerous combinations. Therefore, directly predicting the amplitude and phase of the excitation signal applied to each array antenna port is an understandable solution for diagnosing the array antenna. For this, training was conducted by implementing a regression network for predicting the amplitude and phase of the excitation signal applied to each port. This regression network predicts excitation amplitudes and phases for 16 ports, i.e., values for a total of 32 variables. The extraction environment of the near-field data was similar to that in the classification case. Signals with a random amplitude between 0 and 1 and a random phase between 0 and 360° were excited to 16 ports. Examples of extracted near-field data are shown in Figure 5.

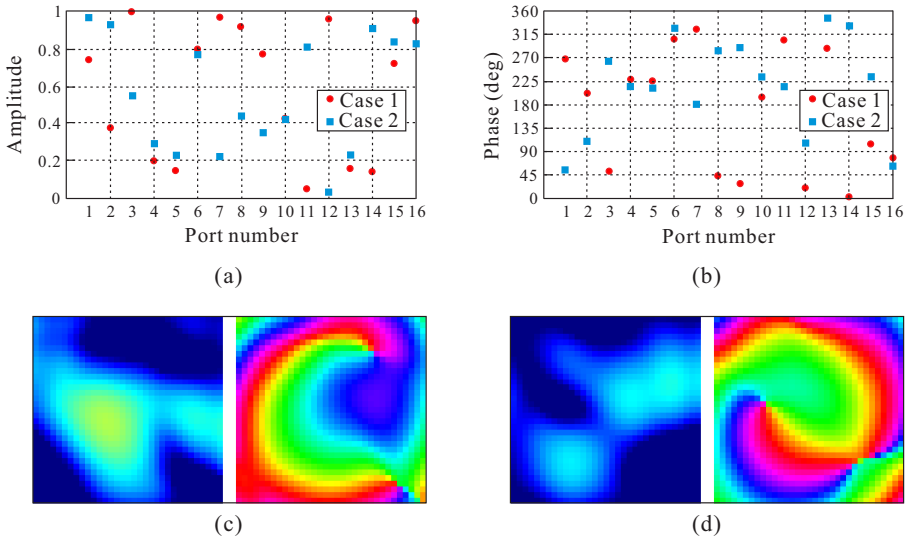

Figure 5. Examples of near-field data based on random excited signal: (**a**) excitation amplitude of ports for cases 1 and 2, (**b**) excitation phase of ports for cases 1 and 2, (**c**) near-field distribution in case 1, and (**d**) near-field distribution in case 2.

A total of 30,000 data were extracted by linking CST MWS and MATLAB. Table 6 lists the accuracies obtained using the test data in the trained regression network as the epoch progresses. Here, accuracy refers to the proportion of the predicted values that are within ±5% of the true values. When a total of 9000 epochs are performed, the training time is 7 days, 16 h, 27 min, and 17 s. The accuracies for amplitude and phase almost converge from 7000 epochs, and accuracies of approximately 95% and 98% are achieved for the excited amplitude and the excited phase, respectively. In order to check the performance of the trained network, the images of cases 1 and 2 shown in Figure 5c,d were applied to the network to predict the amplitude and phase of the signal. Table 7 is a comparison between the true values and the predicted values of cases 1 and 2 applied to the trained regression network. It can be seen that the predicted values are close to the true values. Thus, using this transfer learning method will lead to accurate diagnosis and calibration of array antennas.

Table 6. Training results for the excited signal prediction regression network (6000 test data).

		Epochs					
		4000	**5000**	**6000**	**7000**	**8000**	**9000**
Accuracy (%)	**Amp.**	85.61	88.21	91.20	95.68	96.30	96.20
	Phase	92.69	94.21	96.33	98.30	98.97	98.65
Execution time		3 d 8 h 53 m 21 s	4 d 05 h 36 m 24 s	5 d 1 h 43 m 03 s	5 d 22 h 33 m 13 s	6 d 19 h 33 m 10 s	7 d 16 h 27 m 17 s

Table 7. Comparison between true values and predicted values of cases 1 and 2 applied to regression trained network.

Port Number	Case 1				Case 2			
	Amplitude		Phase (deg)		Amplitude		Phase (deg)	
	True	Pred.	True	Pred.	True	Pred.	True	Pred.
1	0.74	0.78	268	274	0.97	0.93	56	56
2	0.38	0.43	202	198	0.93	0.91	110	120
3	1.00	0.99	52	47	0.55	0.58	265	273
4	0.20	0.16	228	246	0.29	0.24	216	231
5	0.15	0.13	226	209	0.23	0.27	213	227
6	0.80	0.79	305	319	0.77	0.79	328	322
7	0.97	0.98	325	340	0.22	0.22	182	189
8	0.92	0.90	44	55	0.44	0.45	285	274
9	0.77	0.78	29	15	0.35	0.32	290	273
10	0.43	0.45	195	186	0.42	0.42	234	243
11	0.05	0.02	304	298	0.81	0.86	216	216
12	0.96	0.92	20	26	0.03	0.03	107	106
13	0.16	0.14	287	274	0.23	0.23	348	3
14	0.14	0.12	4	12	0.91	0.88	332	336
15	0.72	0.71	106	92	0.84	0.84	234	238
16	0.95	0.95	79	85	0.83	0.84	63	76

3.4. Regression Using Sampling Line of E-Field Data to Reduce the Number of Near-Field Measurement Points

In this study, array antenna diagnosis by transfer learning was conducted by extracting near-field data from the area surrounding the array antenna at a distance of 1λ from a distance of 3λ above the array antenna. However, actual measurements of the near field of the corresponding area require at least several minutes to several tens of minutes. Although the measurement time can be shortened by mechanical improvement of the scanner, there are limitations if the area to be measured is wide. Therefore, we aim to implement a neural network that can diagnose an array antenna using only a few sampling lines without performing near-field measurements for the entire area. As shown in Figure 6, only e-fields of a total of 14 lines were sampled from those of the 34×34 points used in the present training. The data were reconstructed into a 14×34 array, and regression was performed on the excited amplitude and phase of the 4×4 array antenna. Similar to using the near field of the entire area, signals with a random amplitude between 0 and 1 and a random phase of 0 to 360° were excited to 16 ports.

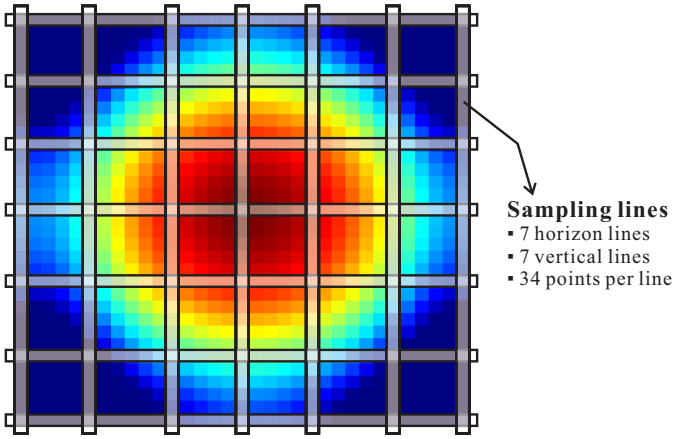

Figure 6. Position of sampling line in the near field.

A total of 30,000 data were used in the regression network, which is similar to the case of using the entire area. Table 8 compares the accuracies obtained using the test data in the trained regression network using a sampling line as the epoch progresses. When a total of 15,000 epochs are performed, the training time is 9 days, 21 h, 41 min, and 49 s. The accuracies almost converge from 13,000 epochs onward, and accuracies of approximately 91% and 96% are achieved for the excited amplitude and the excited phase, respectively. Although the number of near-field points is reduced by more than 58% from the previous 34×34 (1156 points) to 14×34 (476 points), more than 91% accuracy is attained in the prediction of the excited signal of the array antenna.

Table 8. Training results for excited signal prediction regression network using sampling line data (6000 test data, pre-trained network: Alexnet).

		Epochs					
		5000	**7000**	**9000**	**11,000**	**13,000**	**15,000**
Accuracy (%)	**Amp.**	63.58	72.49	77.88	83.91	91.01	90.56
	Phase	70.63	81.26	85.54	91.08	96.22	95.97
Execution time		3 d 14 h 0 m 36 s	4 d 23 h 33 m 21 s	5 d 16 h 58 m 55 s	7 d 02 h 29 m 38 s	8 d 12 h 06 m 41 s	9 d 21 h 41 m 49 s

Table 9 lists the results of the regression network trained in the same environment as above using Resnet-50 as the pre-trained network for comparison according to the type of pre-trained network. When Resnet-50, which is more stable than Alexnet, is used as the pre-trained network, the convergence of the network accuracy occurs in a shorter time than with Alexnet. However, using Alexnet as the pre-trained network leads to slightly higher accuracy than Resnet-50.

Table 9. Training results for excited signal prediction regression network using sampling line data (6000 test data, pre-trained network: Resnet-50).

		Epochs			
		1000	**1500**	**2000**	**2500**
Accuracy (%)	**Amp.**	81.28	92.82	91.05	92.12
	Phase	79.8	93.47	91.91	92.54
Execution time		3 d 11 h 06 m 19 s	5 d 04 h 30 m 43 s	6 d 22 h 07 m 24 s	8 d 15 h 21 m 54 s

4. Validation of Diagnosis Network Using Measurements

Measurements were conducted to validate the proposed near-field-based array antenna diagnosis using transfer learning. The tested array antenna and the measurement environment are shown in Figure 7a,b, respectively. Figure 7c shows the reflection coefficient characteristics of the tested 4×4 array antenna. It consists of four 1×4 series-fed array antennas, which are designed and manufactured to operate in the 5G sub-6 GHz band at 3.55 GHz. Figure 7d displays the shape and S-parameter characteristics of the 1×4 power divider for feeding the tested antenna. It is a Wilkinson power divider, and examination of the S-parameter characteristics shows that it distributes the same power of approximately -7.1 dB at 3.55 GHz to the four ports, and the phases of all ports are similar. For verifying the performance of the fabricated array antenna by near-field measurements, four output ports of the 1×4 power divider and four input ports of the antenna were connected using cables. As the near-field probe, a dielectric rod waveguide probe with low-scattering characteristics was used [17]. The measurement area was 370×370 mm^2, the sampling interval was 10 mm, and the total sampling point was 37×37. To examine the accuracy of the measurements by the near-field probe, a uniform amplitude and phase were supplied to the four input ports of the array antenna, and the measurement was made assuming normal operation. The measured and simulated results are shown in Figure 8. Noticeably, the simulation and measurement distributions are similar.

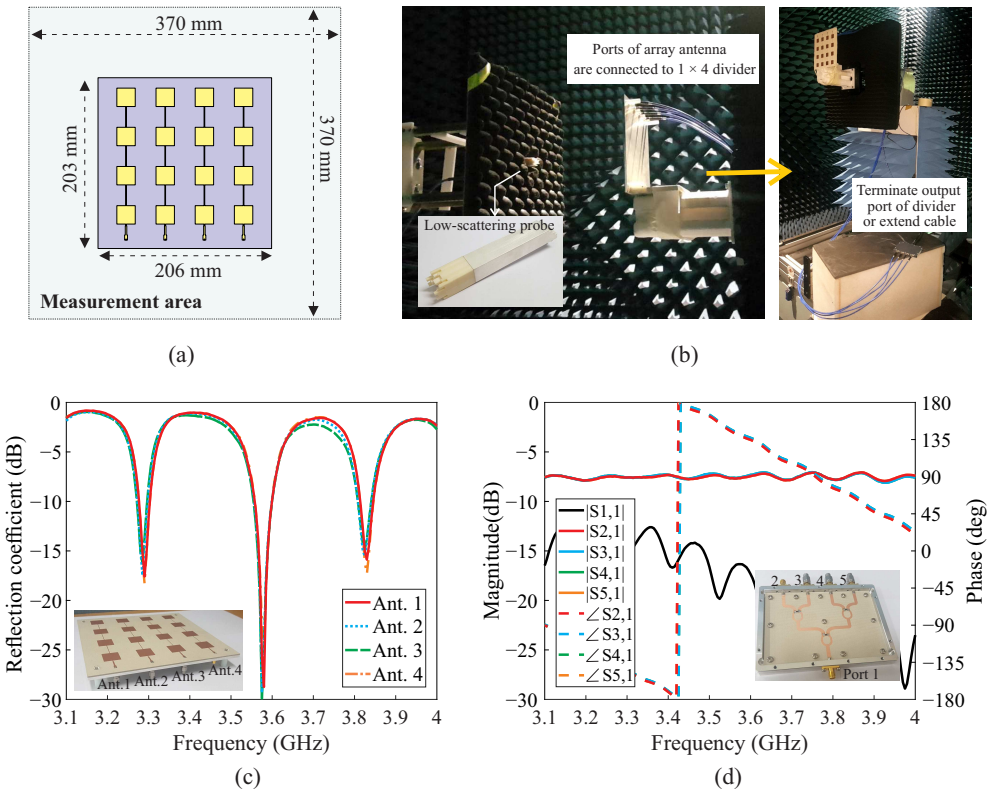

Figure 7. (**a**) Configuration of tested array antenna and measurement information, (**b**) measurement environment, (**c**) measured reflection coefficients of array antenna, and (**d**) measured S-parameters of 1×4 Wilkinson power divider.

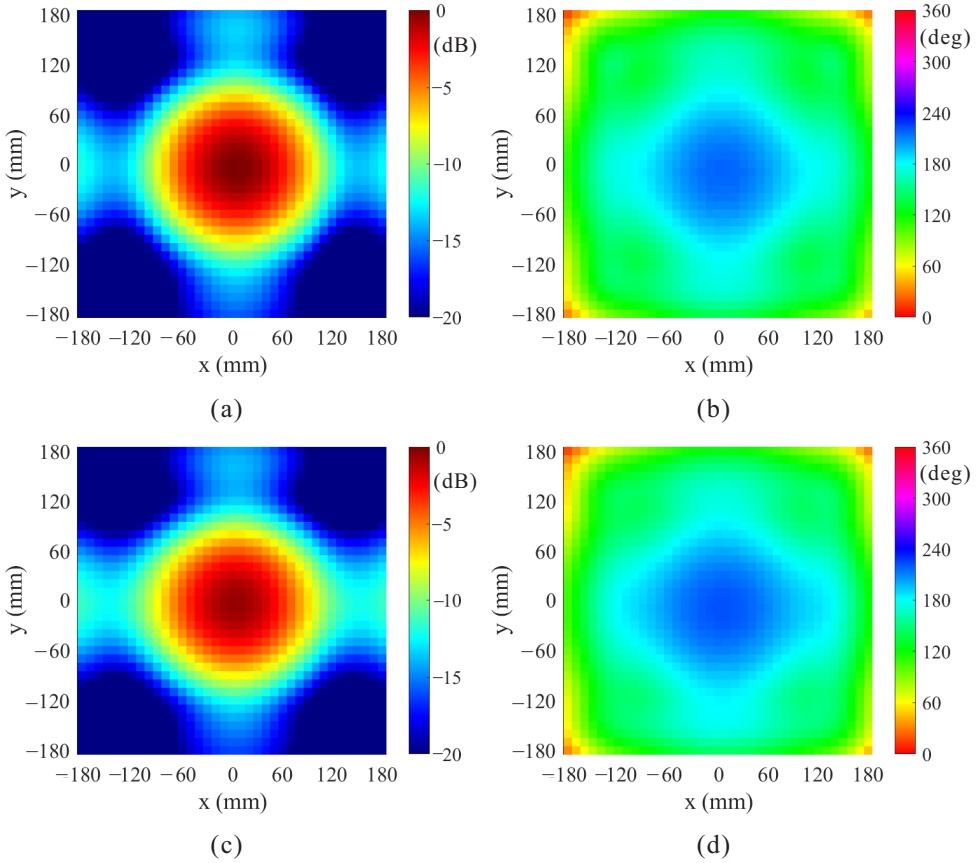

Figure 8. Near-field distribution when applying uniform excitation to ports: (**a**) simulated amplitude, (**b**) simulated phase, (**c**) measured amplitude, and (**d**) measured phase.

Different from the 16-port antenna analyzed by transfer learning, the tested array antenna consists of a 1×4 series feed antenna and is implemented with four ports. Implementation of an array antenna with 16 ports would exponentially increase the number of failure scenarios for each port, making verification by measurement difficult; therefore, an array antenna with four input ports is used. Training for the array antenna diagnosis by measurements was conducted separately. Classes were categorized for a total of 16 cases, assuming normal/abnormal operation for each of the four ports, and training was conducted using 1000 data for each class in the similar environment as in the previous classification. Finally, 98.13% accuracy was achieved with 3200 simulation-based test data. By measuring under various scenarios of array antenna feeding, array antenna diagnosis using a trained network was verified. The scenarios for array antenna diagnosis were assumed by terminating or connecting cables to each input port of the array antenna. The classification of the measurement condition is shown in Table 10. A total of 30 measurements were performed, and the trained network succeeded in discriminating 29 cases and showed an accuracy of 96.67%. The details of the classification network for measurement-based verification are shown in Table 11. These results verify that array antenna diagnosis by transfer learning is feasible.

Table 10. Classification criteria for measurement conditions.

	Measurement Condition		Classification
	Cable Extension	Termination	
Measurement #1	X	X	Pass
Measurement #2	X	Port 1	Port 1 Failure
Measurement #3	Port 3	Port 1	Port 1, 3 Failure
Measurement #4	Port 2, 3	X	Port 2, 3 Failure
…	…	…	…
Measurement #30	Port 1, 3	Port 2, 4	Port 1, 2, 3, 4 Failure

Table 11. Details of a classification network for measurement-based validation.

Classification Network for Measurement-Based Verification	
Applied pre-trained network	Alexnet
Number of sample data	16,000 total data (1000 data per class)
Max epochs	1000
Execution time	1 h 50 m 46 s
Accuracy on simulation-based test data	98.13% (3140/3200)
Accuracy on measurement data	96.67% (29/30)

5. Conclusions

In this study, near-field-based array antenna diagnosis was performed using transfer learning. For a 5G sub-6 GHz band 4×4 array antenna, a network capable of normal/abnormal and specific failure port classifications was implemented, and 99.6% and 95.24% accuracies were achieved, respectively. To improve the accuracy of the array antenna diagnosis, a regression network that predicts the amplitude and phase of the 4×4 array antenna excitation signal was implemented, and the obtained accuracies of the amplitude and phase were 96.2% and 98.65%, respectively. In addition, the array antenna diagnosis by transfer learning was verified by measurements. When the measured data were discriminated using the trained network, accurate discrimination was achieved in 29 out of 30 cases, validating that the array antenna could be diagnosed by transfer learning.

Author Contributions: Conceptualization, H.J.L. and K.C.H.; methodology, H.J.L.; software, H.J.L.; validation, H.J.L., H.B.P. and K.C.H.; formal analysis, H.J.L.; investigation, H.J.L. and D.H.L.; resources, H.J.L. and D.H.L.; data curation, H.J.L. and H.B.P.; writing—original draft preparation, H.J.L.; writing—review and editing, H.J.L., D.H.L. and K.C.H.; visualization, H.J.L; supervision, K.C.H.; project administration, K.C.H. All authors have read and agreed to the published version of the manuscript.

Funding: Not applicable.

Institutional Review Board Statement: Not applicable.

Informed Consent Statement: Not applicable.

Data Availability Statement: Data sharing not applicable.

Conflicts of Interest: The authors declare no conflict of interest.

References

1. Hong, W.; Jiang, Z.H.; Yu, C.; Zhou, J.; Chen, P.; Yu, Z.; Zhang, H.; Yang, B.; Pang, X.; Jiang, M.; et al. Multibeam Antenna Technologies for 5G Wireless Communications. *IEEE Trans. Antennas Propag.* **2017**, *65*, 6231–6249. [CrossRef]
2. Hong, W.; Baek, K.H.; Ko, S. Millimeter-Wave 5G Antennas for Smartphones: Overview and Experimental Demonstration. *IEEE Trans. Antennas Propag.* **2017**, *65*, 6250–6261. [CrossRef]

3. Hansen, R.C. *Phased Array Antennas*, 2nd ed.; John Wiley & Sons, Inc.: Hoboken, NJ, USA, 2009.
4. Aumann, H.M.; Fenn, A.J.; Willwerth, F.G. Phased Array Antenna Calibration and Pattern Prediction Using Mutual Coupling Measurements. *IEEE Trans. Antennas Propag.* **1989**, *37*, 844–850. [CrossRef]
5. Balanis, C.A. *Antenna Theory: Analysis and Design*, 4th ed.; John Wiley & Sons, Inc.: Hoboken, NJ, USA, 2015.
6. Lee, J.J.; Ferren, E.M.; Woollen, D.P.; Lee, K.M. Near-Field Probe Used as a Diagnostic Tool to Locate Defective Elements in an Array Antenna. *IEEE Trans. Antennas Propag.* **1988**, *36*, 884–889. [CrossRef]
7. Gregson, S.; McCormick, J.; Parini, C. *Principles of Planar Near-Field Antenna Measurements*; IET: London, UK, 2007.
8. LeCun, Y.; Boser, B.; Denker, J.S.; Henderson, D.; Howard, R.E.; Hubbard, W.; Jackel, L.D. Backpropagation applied to handwritten zip code recognition. *Neural Comput.* **1989**, *1*, 541–551. [CrossRef]
9. Russakovsky, O.; Deng, J.; Su, H.; Krause, J.; Satheesh, S.; Ma, S.; Huang, Z.; Karpathy, A.; Khosla, A.; Bernstein, M.; et al. ImageNet Large Scale Visual Recognition Challenge. *Int. J. Comput. Vis.* **2015**, *115*, 211–252. [CrossRef]
10. Torrey, L.; Shavlik, J. *Transfer Learning*; IGI Global: Hershey, PA, USA, 2010.
11. Kermany, D.S.; Goldbaum, M.; Cai, W.; Valentim, C.C.; Liang, H.; Baxter, S.L.; McKeown, A.; Yang, G.; Wu, X.; Yan, F.; et al. Identifying Medical Diagnoses and Treatable Diseases by Image-Based Deep Learning. *Cell* **2018**, *172*, 1122–1131. [CrossRef] [PubMed]
12. Feng, C.; Zhang, H.; Wang, S.; Li, Y.; Wang, H.; Yan, F. Structural Damage Detection using Deep Convolutional Neural Network and Transfer Learning. *KSCE J. Civil Eng.* **2019**, *23*, 4493–4502. [CrossRef]
13. Kaya, A.; Keceli, A.S.; Catal, C.; Yalic, H.Y.; Temucin, H.; Tekinerdogan, B. Analysis of Transfer Learning for Deep Neural Network Based Plant Classification Models. *Comput. Electron. Agric.* **2019**, *158*, 20–29. [CrossRef]
14. Krizhevsky, A.; Sutskever, I.; Hinton, G.E. ImageNet Classification with Deep Convolutional Neural Networks. In Proceedings of the 25th International Conference on Neural Information Processing Systems, Lake Tahoe, NV, USA, 3–6 December 2012; pp. 1106–1114.
15. He, K.; Zhang, X.; Ren, S.; Sun, J. Deep Residual Learning for Image Recognition. In Proceedings of the IEEE Conference on Computer Vision and Pattern Recognition, Las Vegas, NV, USA, 27–30 June 2016; pp. 770–778.
16. Trinh-Van, S.; Hwang, K.C. Miniaturised Broadband Top-Loaded Planar Monopole Antenna with Binary-Encoded Sleeves. *Electron. Lett.* **2015**, *51*, 958–970. [CrossRef]
17. Lim, H.J.; Park, H.B.; Hwang, K.C. A Low-Scattering Pixelated Dielectric Rod Waveguide Probe for Near-Field Measurements. *IEEE Trans. Antennas Propag.* **2021**. [CrossRef]